Philippine Journal of Science
147 (4): 639-646, December 2018
ISSN 0031 - 7683
Date Received: 20 Feb 2018

Infrared and Raman Microscopy of the Arsenate Double Salt Mineral Tilasite, $CaMg(AsO_4)F$, from Långban, Värmland, Sweden

J. Theo Kloprogge[1,2]

[1]Department of Chemistry, College of Arts and Sciences,
The University of the Philippines Visayas, Miag-ao, Iloilo 5023 Philippines
[2]School of Earth and Environmental Sciences, The University of Queensland,
Brisbane 4072 Queensland, Australia

This paper aims at a full description of the Raman and Infrared spectra of the arsenate mineral tilasite, $CaMg(AsO_4)F$, from Långban, Värmland, Sweden. X-ray diffraction showed the two samples to be phase pure with a monoclinic unit cell of a = 6.683(3) Å, b = 8.950(5) Å, c = 7.572(4) Å, and β = 121.09(2)°. The infrared and Raman spectra were dominated by the arsenate modes. The two highest intensity bands were observed at 850 cm^{-1} and 831 cm^{-1} and were assigned to the Raman active ν_1 symmetric stretching vibration (A_1) and the Raman active triply degenerate ν_3 antisymmetric stretching vibration (F_2). The Raman and infrared active triply degenerate ν_3 antisymmetric stretching vibration (F_2) was observed in the infrared spectrum at 822 cm^{-1}, 792 cm^{-1}, and 761 cm^{-1}. The intense Raman band at 465 cm^{-1} was assigned to the Raman active triply degenerate ν_4 bending vibration (F_2). The corresponding infrared bands were observed at 523 cm^{-1}, 449 cm^{-1}, and 414 cm^{-1}. The intense Raman band at 329 cm^{-1} was attributed to the Raman active doubly degenerate ν_2 symmetric bending vibration (E). Lowering of the symmetry of the tetrahedral arsenate group led to significant splitting of these modes. The low wave number region below 320 cm^{-1} was assigned to metal-oxygen stretching and lattice vibrations. In the range of 1000–1100 cm^{-1}, four very weak bands were observed. These bands were probably due to the $\nu_3(F_2)$ of a very small amount of phosphate substituted for arsenate in the crystal structure of tilasite.

Key words: arsenate, infrared spectroscopy, Raman spectroscopy, tilasite

INTRODUCTION

Tilasite was originally described by Sjögren (1895) from Långban, Värmland, Sweden. The name honours Daniel Tilas (1712–1772), a Swedish mining engineer and mineral collector of Stockholm, Sweden. The crystal structure was found to be similar to that of titanite $CaTiSiO_5$ by Bladh *et al*. (1972) as earlier predicted by Strunz (1937). They used fragments of tilasite from Bisbee, AZ, USA, to determine the crystal structure with the position of the Mg correlating to that of the octahedral Ti site in titanite. The arsenate groups were analogous to the silica tetrahedra and the fluoride ions occupied the same sites as the non-tetrahedral oxygen atoms in titanite. The arsenate group was approximately tetrahedral with As–O distances ranging 1.65–1.72 Å and O–As–O angles varying 104.1–113.9°. The Mg atom is in a slightly distorted octahedral coordination of 4 O atoms and 2 F atoms. The Ca atom is seven coordinated in the tilasite structure. In a single crystal study, Bermanec (1994) determined that the space group was $C2/c$ rather than Cc as determined by Bladh *et al*. (1972), confirming the attribution of Richmond (1940) for tilasite ($C_{2h}^6 - C2/c$).

*Corresponding author: j.kloprogge@uq.edu.au

The observed pyroelectric effects were considered to be anomalous rather than symmetry-related (Bermanec 1994). Tilasite forms a continuous series with durangite [$NaAl(AsO_4)F$] and maxwellite [$NaFe^{3+}(AsO_4)F$], a group of anhydrous arsenate minerals with an additional anion. All three minerals are monoclinic. Tilasite is isostructural with lacroixite ($NaAlPO_4F$) and isokite ($CaMgPO_4F$). For tilasite, the cell parameters are a = 7.553 Å, b = 8.951 Å, c = 6.701 Å, Z = 4, β = 120.967°, and V = 388.46 (Bladh *et al*. 1972). This was later changed to a = 6.681–6.701 Å, b = 8.950–8.944 Å, c = 7.552–7.573 Å, β = 120°58'–121°14', and Z = 4 (Anthony *et al*. 1990). Tilasite typically occurs in metamorphosed manganese or zinc deposits containing arsenic (*e.g*., Aminoff 1923, Bermanec 1994, Borisovskii *et al*. 1984, Brugger & Giere 1999, Graeser & Roggiani 1978, Lorenz 1995, Parker & Peters 1978, Sjögren 1895, Smith & Prior 1912, Williams 1970).

Myneni *et al*. (1998a, 1998b) and Nakamoto (2009) reported that since $(AsO_4)^{3-}$ is a tetrahedral unit, it will exhibit four fundamental vibrations *i.e*., the Raman active ν_1 symmetric stretching vibration (A_1) around 818 cm^{-1}, the Raman active doubly degenerate ν_2 symmetric bending vibration (E) around 350 cm^{-1}, the infrared and Raman active triply degenerate ν_3 antisymmetric stretching vibration (F_2) around 786 cm^{-1}, and the infrared and Raman active triply degenerate ν_4 bending vibration (F_2) around 405 cm^{-1}. Protonation, metal complexation, and/or adsorption on a mineral surface will cause the change in $(AsO_4)^{3-}$ symmetry from T_d to lower symmetries, such as C_{3v}/C_3 (corner sharing); C_{2v}/C_2 (edge sharing, bidentate binuclear); or even C_1/C_s (corner sharing, edge sharing, bidentate binuclear, multidentate) (Myneni *et al*. 1998a, 1998b). This loss of degeneracy causes splitting of degenerate vibrations of $(AsO_4)^{3-}$ and the shifting of the As–O stretching vibrations to different wavenumbers. Accompanying the $(AsO_4)^{3-}$ symmetry and coordination changes, the A_1 band might move to higher or lower wavenumbers and the doubly degenerate E and triply degenerate F modes may result in several new A_1, B_1, and/or E vibrations (Myneni *et al*. 1998a, 1998b).

Raman and infrared spectroscopy have proven very useful for the study of minerals. Raman spectroscopy has proven most useful for the study of diagenetically and structurally related minerals such as minerals containing sulfate, arsenate, and/or phosphate groups. This paper is a continuation of systematic studies of infrared and Raman spectroscopy of minerals of secondary origin generally occurring in the oxide supergene zone (*e.g*., Frost *et al*. 2005, 2007, Kloprogge & Frost 1999, 2000; Kloprogge *et al*. 2006, Kloprogge & Wood 2017a, 2017b; Martens *et al*. 2003, 2004a, 2004b). Frost *et al*. (2014) – in their study of maxwellite – used tilasite for comparison, but a completely satisfactory analysis and interpretation of the Raman and infrared spectra of tilasite was not provided. Therefore, in this work, a thorough interpretation of the infrared and Raman spectra of two pure tilasite samples is attempted. The observed bands are attributed to the different vibrational modes of tilasite in relation to its structure.

MATERIALS AND METHODS

Samples

Two samples of tilasite from the private collection of the author were used for this study (micromount collection catalogue nos. 7510 and 2379). Both samples are from the type locality Långban, Värmland, Sweden and consist of violet to pinkish crystals in matrix.

Sample Analysis

The nature of the crystals was determined by X-ray diffraction (XRD) prior to the spectroscopic analyses. XRD patterns of the powdered samples were recorded on a Philips wide-angle PW1050/25 vertical goniometer applying Cu Kα radiation. The samples were measured at 50% RH in stepscan mode with steps of 0.01°2θ and a scan speed of 1.00° min^{-1} from 5°2θ to 75°2θ. The unit cell was refined using the Rietveld method using the software supplied with the XRD instrument. X-ray photoelectron spectroscopy (XPS) analyses were performed on a Kratos AXIS Ultra with a monochromatic Al X-ray source at 225 W under ultra-high vacuum conditions. Each analysis included a survey scan at 0–1200 eV with a dwell time of 100 ms and pass energy of 160 eV at steps of 1 eV with 1 sweep. The spectra were charge corrected using the advantageous C 1s signal at 284.8 eV. The sample with the crystal *in situ* was placed in the XPS after a wash with alcohol. Prior to the analyses, the surface of the crystal was cleaned by etching for 20 min. The FTIR microscopic spectrum of the tilasite sample no. 7510 was obtained using a Perkin Elmer 2000 *i*-series FT–IR microscope. Spectra of 4 cm^{-1} resolution within 4000–400 cm^{-1} were acquired by coaddition of 128 scans. For Raman spectroscopic measurements the samples were orientated on the stage of an Olympus BHSM microscope equipped with 10x and 50x objectives. The microscope is part of a Renishaw 1000 Raman microscope system, which also includes a monochromator, a filter system, and a charge-coupled device. Raman spectra were excited by a HeNe laser (633 nm) at a nominal resolution of 2 cm^{-1} and collected over the range of 200–4000 cm^{-1}. Repeated acquisition using the highest magnification was accumulated to improve the signal to noise ratio. The grating of the Raman microspectrometer was calibrated using the 520.5 cm^{-1} line of silicon wafer. Spectroscopic

manipulation such as baseline adjustment, smoothing and normalization, and band component analysis was undertaken using the Fytik 0.9.8 software package (Wojdyr 2010), which enabled the type of fitting, function to be selected and allows specific parameters to be fixed or varied accordingly. Band fitting was done using a Gauss-Lorentz cross-product function with the minimum number of component bands used for the fitting process. The Gauss-Lorentz ratio was maintained at values greater than 0.7 and fitting was undertaken until reproducible results were obtained with squared correlations of r^2 greater than 0.995.

RESULTS AND DISCUSSION

The XRD pattern of one of the two samples (no. 7510) is shown in Figure 1. The pattern is consistent with that of pure tilasite. A similar result was obtained for the other sample. The unit cell was calculated based on the monoclinic crystal system with a = 6.683(3) Å, b = 8.950(5) Å, c = 7.572(4) Å, and β = 121.09(2)°. Table 1 provides an overview of the observed and calculated d-values, intensities (strongest reflection = 100) and the corresponding hkl Miller indices. The chemical compositions of the two samples based on XPS survey scans are listed in Table 2. Both samples show a nearly identical composition (within instrumental error) close to the ideal composition for tilasite with only trace amounts of Fe, Mn, and P.

The infrared spectrum of tilasite as shown in Figure 2 is characterized by broad bands, while the bands in the corresponding Raman spectra are much sharper. The two samples showed minor differences in intensity as a result of the orientation of the tilasite crystal under the laser beam in the Raman microscope. The band positions, however, are very similar. These spectra exhibit the positions and

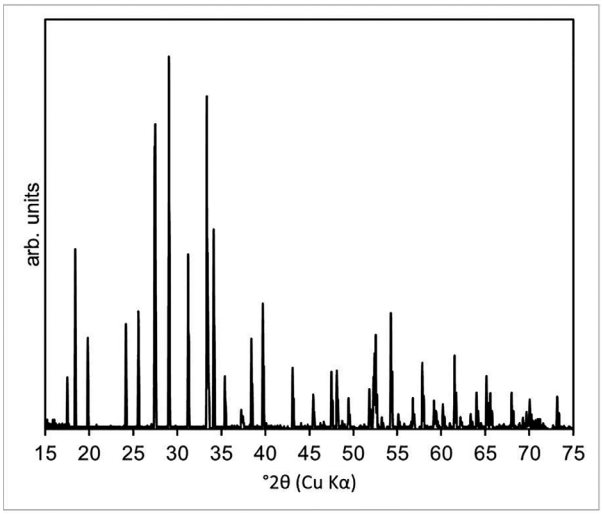

Figure 1. XRD pattern of tilasite, sample no. 7510.

relative intensities of the infrared and Raman bands for the two samples. Since large parts of the spectra show no intensity, the spectra were subdivided into regions based upon the type of molecular vibration being studied.

In the infrared spectrum of tilasite, the broad infrared bands overlap; however, band component analysis allows the component bands to be resolved. In the range of 1000–1100 cm^{-1}, four very weak bands were observed (Figure 3a). Similar bands were also visible in the infrared spectrum reported in the online RRUFF mineral spectral database (RRUFF Project). These bands are probably the $\nu_3(F_2)$ of a very small amount of phosphate substituted for arsenate in the crystal structure of tilasite. Anthony *et al*. (1990) reported 0.10 wt% P_2O_5 in tilasite from Långban. These bands were not reported by Frost *et al*. (2014).

Table 3 provides a complete overview of the band component analysis of both the infrared and Raman spectra in comparison to the results provided by Frost *et*

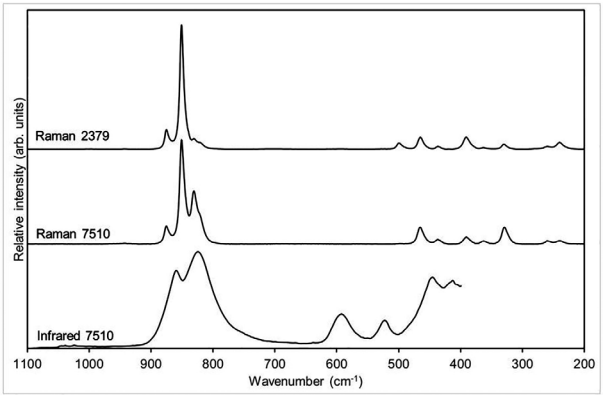

Figure 2. Infrared and Raman spectra of the two tilasite samples no. 7510 and 2379 in the region between 1100 cm^{-1} and 200 cm^{-1}.

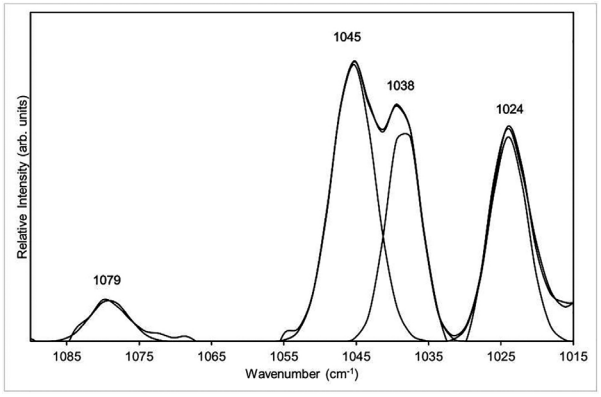

Figure 3a. Band component analysis of the infrared spectrum of tilasite between 1090 cm^{-1} and 1015 cm^{-1}.

Table 1. XRD cell refinement data with 2θ in degrees, d-values in Å, and intensities based on strongest line having intensity of 100.

	Observed	Calculated	Difference				
2θ	**d_{obs}**	**d_{calc}**	**d_{obs}–d_{calc}**	**Intensity**	**h**	**k**	**l**
17.49	5.070597	5.071285	–0.000688	13.74	–1	1	1
18.39	4.824424	4.825644	–0.001220	48.35	1	1	0
19.83	4.477220	4.478776	–0.001556	24.51	0	2	0
24.15	3.685224	3.685435	–0.000211	28.28	0	2	1
25.57	3.483700	3.484313	–0.000613	31.66	–1	1	2
29.03	3.075882	3.076098	–0.000216	100.00	–2	0	2
31.22	2.864934	2.863943	0.000991	47.00	2	0	0
33.35	2.686667	2.686202	0.000465	89.43	–1	3	1
34.13	2.627031	2.626649	0.000382	53.61	0	2	2
35.40	2.535642	2.535642	0.000000	14.19	–2	2	2
38.41	2.343582	2.343566	0.000016	24.26	–1	3	2
39.71	2.269806	2.268915	0.000891	33.70	1	3	1
43.10	2.098807	2.098612	0.000195	16.50	–3	1	1
45.44	1.996020	1.995187	0.000833	9.31	2	2	1
46.64	1.947424	1.946963	0.000461	1.99	0	2	3
47.51	1.913774	1.913532	0.000242	15.45	–1	3	3
48.12	1.890930	1.891087	–0.000157	15.77	–2	0	4
49.45	1.843142	1.842718	0.000424	8.35	0	4	2
51.81	1.764600	1.764115	0.000485	10.75	2	4	0
54.27	1.690283	1.690428	-0.000145	31.21	–3	3	3
56.76	1.621905	1.621441	0.000464	8.37	0	0	4
57.84	1.594165	1.593823	0.000342	17.85	1	5	1
60.18	1.537656	1.538049	–0.000393	6.75	–4	0	4
61.50	1.507783	1.507392	0.000391	19.79	1	3	3
64.00	1.454786	1.454768	0.000018	9.87	–1	5	3
67.99	1.378806	1.378598	0.000208	9.84	–3	5	1
70.05	1.343219	1.343101	0.000118	7.97	–2	6	2
73.17	1.293456	1.293364	0.000092	8.76	–1	3	5

Table 2. Chemical composition of tilasite, $CaMg(AsO_4)F$, based on XPS survey scans.

Cation	Normalized 4O	XPS at % sample no. 7510	XPS at % sample no. 2379	Normalized 4O sample no. 7510	Normalized 4O sample no. 2379
Ca	1	14.0	14.0	0.96	0.97
Mg	1	13.8	14.1	0.97	0.97
Fe	0	<0.1*	<0.1*	<0.01	<001
Mn	0	<0.1*	-	<0.01	-
F	1	13.7	13.9	0.96	0.96
P	0	<0.1*	<0.1*	<0.01	<0.01
O	4	58.1	57.9	4.00	4.00
Total		99.6	99.9		

Table 3. Comparison of infrared and Raman band positions (in cm^{-1}) plus tentative vibrational mode assignments.

Infrared, this study	Infrared, Frost *et al*. (2014)	Raman, this study	Raman, Frost *et al*. (2014)	Raman, RRUFF Project	Vibrational mode
	3437				H_2O OH-stretch
	3196				H_2O OH-stretch
	1667				H_2O OH bend
1079					$\nu_3(F_2)$ PO_4
1045					$\nu_3(F_2)$ PO_4
1038					$\nu_3(F_2)$ PO_4
1024					$\nu_3(F_2)$ PO_4
882	896	875	875	874	ν_1 sym. stretching AsO_4
861	858	855	859	850	ν_1 sym. stretching AsO_4
			851		ν_1 sym. stretching AsO_4
838	841	843	843	842	ν_1 sym. stretching AsO_4
		831	831	830	ν_1 sym. stretching AsO_4
822	819	822	820	821	ν_3 antisym. stretching vibration AsO_4
792	789				ν_3 antisym. stretching vibration AsO_4
761	769				ν_3 antisym. stretching vibration AsO_4
	739				ν_3 antisym. stretching vibration AsO_4
593					?
523		499	501	501	ν_4 bending vibration AsO_4
		490	494	490	ν_4 bending vibration AsO_4
		481		482	ν_4 bending vibration AsO_4
		465	467	463	ν_4 bending vibration AsO_4
449		454	450	455	ν_4 bending vibration AsO_4
431		436	438	432	ν_4 bending vibration AsO_4
414					ν_4 bending vibration AsO_4
		390	393	388	ν_2 sym. bending vibration AsO_4
		380		380	ν_2 sym. bending vibration AsO_4
		363	365	360	ν_2 sym. bending vibration AsO_4
		329	331	327	ν_2 sym. bending vibration AsO_4
		319			M-O stretch
		259	261	255	M-O stretch
		240	243	243	M-O stretch
		194	197		M-O stretch
		186			M-O stretch
		155	160		Lattice vibration
		145	149		Lattice vibration
			139		Lattice vibration
		125			Lattice vibration
		118	111		Lattice vibration

al. (2014) and in the RRUFF online database of mineral spectra (RRUFF Project). The region within 750–900 cm^{-1} in both the infrared and Raman spectra show a series of bands associated with the AsO_4 group in the crystal structure (Figures 3b and 4). Shoulder bands within 820–843 cm^{-1} are probably also due to this vibrational mode. The fact that this Raman active mode in perfect tetrahedral AsO_4, is also observed in the infrared spectrum at 861 cm^{-1} indicates a lowering of the symmetry, allowing this mode to become infrared active. The Raman active bands at 875 cm^{-1} and 855 cm^{-1} (associated with similar bands in the infrared at 882 cm^{-1} and 861 cm^{-1}) were attributed by Frost *et al*. (2014) to ν_{sym} and ν_{asym} of $(AsO_3F)^{2-}$ groups in the crystal structure. However, in the crystal structure, these groups do not occur. The fluorine atom takes up a separate position besides the AsO_4 groups. It is more likely that these bands are also associated with the ν_1 symmetric stretching vibration (A_1). The Raman and infrared active triply degenerate ν_3 antisymmetric stretching vibration (F_2) is observed in the infrared spectrum at 822 cm^{-1}, 792 cm^{-1}, and 761 cm^{-1}.

The origin of the infrared band at 593 cm^{-1} is not clear at this point in time, although a possible interpretation is that this is a Mg–O or Mg–F stretching vibration (Figure 3c). The intense Raman band at 465 cm^{-1} is assigned to the Raman active triply degenerate ν_4 bending vibration (F_2) (Figure 5). The other low intensity Raman bands at 436 cm^{-1}, 454 cm^{-1}, 490 cm^{-1}, and 499 cm^{-1} of tilasite are probably due to this vibration caused by a reduction of the symmetry of the arsenate anion in the tilasite structure. The corresponding infrared bands are observed at 523 cm^{-1}, 449 cm^{-1}, and 414 cm^{-1}. The intense Raman band at 329 cm^{-1} is attributed to the Raman active doubly degenerate ν_2 symmetric bending vibration (E). The two other Raman bands at 363 cm^{-1} and 390 cm^{-1} are also assigned to this vibration.

The low wavenumber regions are shown in Figures 5 and 6. Intense Raman bands are present at 319 cm^{-1} with low intensity bands at 259 cm^{-1}, 240 cm^{-1}, 194 cm^{-1}, and 186 cm^{-1}. It is thought that these bands are due to metal oxygen stretching vibrations. The remaining bands at 155 cm^{-1}, 145 cm^{-1}, 125 cm^{-1}, and 118 cm^{-1} are interpreted as lattice vibrations.

The OH-stretching and bending vibrations observed by Frost *et al*. (2014) in their supplementary material was not observed in the spectrum of tilasite in this study. A major problem with their study is the lack of characterization of the material prior to the Raman and infrared spectroscopy. No information is provided on the locality of the sample except for a general referral to Anthony *et al*. (1990). No XRD was recorded nor was any energy-dispersive X-ray spectroscopy work done (as was for the maxwellite in the same study). Therefore, the observation of OH-bands (both M–OH stretching and OH-stretching and bending modes of water) may simply be due to other minerals in their powdered sample.

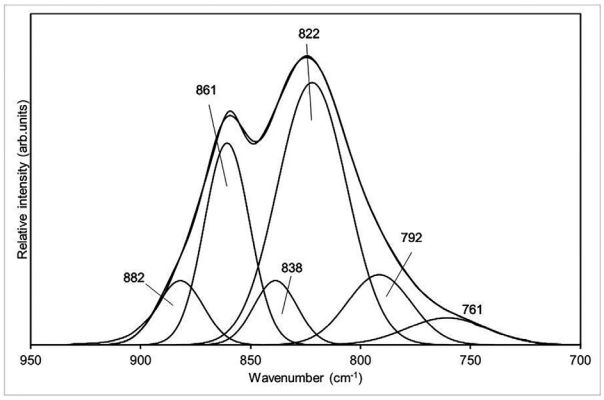

Figure 3b. Band component analysis of the infrared spectrum of tilasite between 950 cm^{-1} and 700 cm^{-1}.

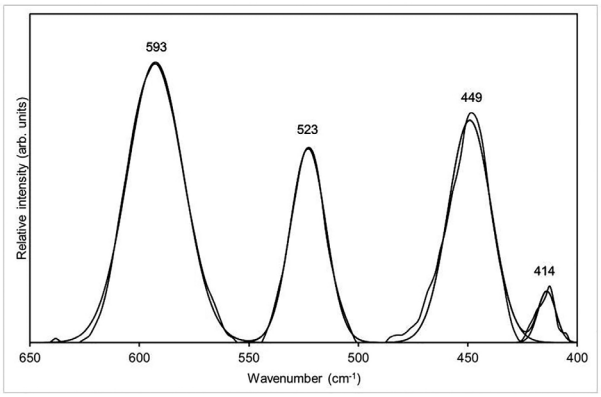

Figure 3c. Band component analysis of the infrared spectrum of tilasite between 650 cm^{-1} and 400 cm^{-1}.

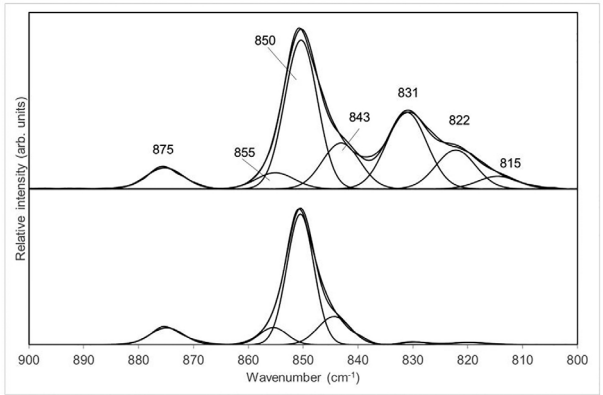

Figure 4. Band component analysis of the Raman spectra in the region between 900 cm^{-1} and 800 cm^{-1} for tilasite sample no. 7510 (top) and sample no. 2379 (bottom).

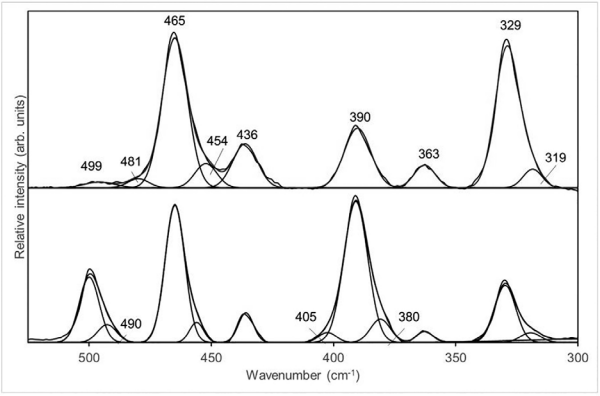

Figure 5. Band component analysis of the Raman spectra in the 525–300 cm^{-1} region of tilasite sample no. 7510 (top) and sample no. 2379 (bottom).

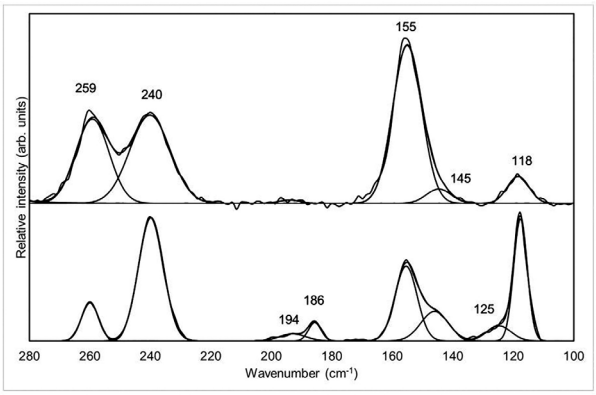

Figure 6. Band component analysis of the Raman spectra in the 280–100 cm^{-1} region of tilasite sample no. 7510 (top) and sample no. 2379 (bottom).

CONCLUSIONS

A combination of XRD and both Raman and infrared microscopy were used to study the chemistry and molecular structure of the mineral tilasite, $CaMg(AsO_4)F$. XRD showed the phase purity of both samples used in this study. The molecular structure of tilasite was analysed by Raman and infrared spectroscopy. Raman and infrared bands were assigned to the different AsO_4 stretching and bending vibrations, as well as the structural metal-oxygen and lattice modes. Overall, the Raman spectra were very similar to those reported in the RRUFF database (RRUFF Project). No bands attributable to water or hydroxyl stretching vibrations were observed, in contrast to the results of Frost *et al*. (2014) thatwere based on an insufficiently characterized sample without any XRD or chemical analysis and of unknown origin.

ACKNOWLEDGMENTS

The author thanks the School of Chemistry, Physics, and Mechanical Engineering, QUT, Brisbane, for the use of the equipment for this study. The author acknowledges the facilities and the scientific and technical assistance of the Australian Microscopy & Microanalysis Research Facility at the Centre for Microscopy and Microanalysis, The University of Queensland.

REFERENCES

AMINOFF G. 1923. The mineral tilasite at Långban. Geologiska Foereningens i Stockholm Foerhandlingar 45: 144–159.

ANTHONY JW, BIDEAUX RA, BLADH KW, C. NM. 1990. Tilasite. In: Handbook of Mineralogy. Tucson Arizona, USA: Mineral Data Publishing.

BERMANEC V. 1994. Centro-symmetric tilasite from Nežilovo, Macedonia: A crystal structure refinement. Neues Jahrbuch fuer Mineralogie Monatshefte 170(7): 289–294.

BLADH KW, CORBETT RK, MCLEAN WJ, LAUGHON RB. 1972. Crystal structure of tilasite. American Mineralogist 57: 1880–84.

BORISOVSKII SE, REZNIKOV NV, BASOVA GV. 1984. First occurrence of tilasite in the USSR. Doklady Akademii Nauk SSSR 276: 223–227.

BRUGGER J, GIERE R. 1999. As, Sb, Be and Ce enrichment in minerals from a metamorphosed Fe–Mn deposit, Val Ferrera, eastern Swiss Alps. Canadian Mineralogist 37: 37–52.

FROST RL, SCHOLZ R, LOPEZ A, XI Y. 2014. Raman spectroscopy of the arsenate minerals maxwellite and in comparison with tilasite. Spectrochimica Acta Part A: Molecular and Biomolecular Spectroscopy 123: 416–420.

FROST RL, WEIER ML, KLOPROGGE JT, RULL F, MARTINEZ-FRIAS J. 2005. Raman spectroscopy of halotrichite from Jaroso, Spain. Spectrochimica Acta Part A: Molecular and Biomolecular Spectroscopy 62A: 176–180.

FROST RL, WEIER ML, WILLIAMS PA, LEVERETT P, KLOPROGGE JT. 2007. Raman spectroscopy of the sampleite group of minerals. Journal of Raman Spectroscopy 38: 574–583.

GRAESER S, ROGGIANI AG. 1978. Tilasite of the Pizzo Cervandone (Valle Devero, Ossola). New minerals for Italy. Rendiconti della Societa Italiana di Mineralogia

e Petrologia 34: 51–53.

KLOPROGGE JT, DUONG LV, WEIER M, MARTENS WN. 2006. Nondestructive identification of arsenic and cobalt minerals from Cobalt City, Ontario, Canada: arsenolite, erythrite, and spherocobaltite on pararammelsbergite. Applied Spectroscopy 60: 1293–96.

KLOPROGGE JT, FROST RL. 1999. A Raman microscopic study of tungstate and molybdate minerals: Scheelite, wolframite and wulfenite. Neues Jahrbuch fuer Mineralogie Monatshefte 5(5): 193–211.

KLOPROGGE JT, FROST RL. 2000. Raman microscopy study of tyrolite: A multi-anion arsenate mineral. Applied Spectroscopy 54: 517–521.

KLOPROGGE JT, WOOD BJ. 2017a. X-ray Photoelectron Spectroscopic and Raman microscopic investigation of the variscite group minerals: Variscite, strengite, scorodite and mansfieldite. Spectrochimica Acta Part A: Molecular and Biomolecular Spectroscopy 185: 163–172.

KLOPROGGE JT, WOOD BJ. 2017b. X-ray Photoelectron spectroscopic and Raman spectroscopic study of bayldonite from Wheal Carpenter, Cornwall, UK. Vacuum. 141: 49–56.

LORENZ J. 1995. Minerals in the rhyolite quarry of Sailauf including new discoveries of native arsenic, bertrandite, humboldtine and tilasite. Aufschluss 46: 105–122.

MARTENS WN, FROST RL, KLOPROGGE JT, WILLIAMS PA. 2003. The basic copper arsenate minerals olivenite, cornubite, cornwallite, and clinoclase: An infrared emission and Raman spectroscopic study. American Mineralogist 88: 501–508.

MARTENS WN, KLOPROGGE JT, FROST RL, RINTOUL L. 2004a. Single-crystal Raman study of erythrite, $Co_3(AsO_4)_2 \cdot 8H_2O$. Journal of Raman Spectroscopy 35: 208–216.

MARTENS WN, RINTOUL L, KLOPROGGE JT, FROST RL. 2004b. Single crystal Raman spectroscopy of cerussite. American Mineralogist 89: 352–358.

MYNENI SCB, TRAINA SJ, WAYCHUNAS GA, LOGAN TJ. 1998a. Experimental and theoretical vibrational spectroscopic evaluation of arsenate coordination in aqueous solutions, solids, and at mineral-water interfaces. Geochimica et Cosmochimica Acta 62: 3285–3300.

MYNENI SCB, TRAINA SJ, WAYCHUNAS GA, LOGAN TJ. 1998b. Vibrational spectroscopy of functional group chemistry and arsenate coordination in ettringite. Geochimica et Cosmochimica Acta 62: 3499–3514.

NAKAMOTO K. 2009. Infrared and Raman Spectra of Inorganic and Coordination Compounds. 6th ed. New York: Wiley.

PARKER FJ, PETERS TA. 1978. Tilasite from the Sterling Hill mine, Ogdensburg, New Jersey [USA]. Mineralogical Record 9: 385–386.

RICHMOND WE. 1940. Crystal chemistry of the phosphates, arsenates and vanadates of the type $A_2XO_4(Z)$. American Mineralogist 25: 441–478.

RRUFF PROJECT. Retrieved from http://rruff.info/tilasite/display=default/R050246 on 22 Jun 2018.

SJÖGREN H. 1895. Preliminära meddelanden om några undersökningar på svenska mineral. 4. Tilasit eller fluor-adelit från Långban. Geologiska Föreningens i Stockholm Förhandlingar 17: 291–294.

SMITH GFH, PRIOR GT. 1912. Fermorite, a New Arsenate and Phosphate of Lime and Strontia and Tilasite from the Manganese Ore Deposits of India. Mineralogical Magazine 16: 84–97.

STRUNZ H. 1937. Titanite and tilasite. Zeitschrift fuer Kristallographie, Kristallgeometrie, Kristallphysik, Kristallchemie 96: 7–14.

WILLIAMS SA. 1970. Tilasite from Bisbee, Arizona. Mineralogical Record 1: 68–69.

WOJDYR M. 2010. Fityk: A general-purpose peak fitting program. Journal of Applied Crystallography 43: 1126–28.